

Landau Levels on a Surface of Weak Topological Insulators

Yositake Takane

*Department of Quantum Matter, Graduate School of Advanced Sciences of Matter,
Hiroshima University, Higashihiroshima, Hiroshima 739-8530, Japan*

(Received)

A three-dimensional weak topological insulator (WTI), being equivalent to stacked layers of two-dimensional quantum spin-Hall insulators, accommodates massless Dirac electrons on its side surface. A notable feature of WTIs is that surface states typically consist of two Dirac cones in the reciprocal space. We study the Landau quantization of Dirac electrons of WTIs in a perpendicular magnetic field. It is shown that when the magnetic length l_B is much larger than the interlayer distance a , surface electrons are quantized into Landau levels according to the ordinary quantization rule for Dirac electrons. It is also shown that, with decreasing l_B toward a , each Landau level and its spin state become modulated in a nontrivial manner. We demonstrate that this is attributed to the mixing of two Dirac cones induced by the discreteness of the layered structure.

1. Introduction

Three-dimensional (3D) weak topological insulators (WTIs) can be regarded as stacked layers of two-dimensional (2D) quantum spin-Hall (QSH) insulators.^{1–3)} The stacking direction is designated by the weak vector $\boldsymbol{\nu} \equiv (\nu_1\nu_2\nu_3)$ with ν_1 , ν_2 , and ν_3 being weak indices. As a 2D QSH insulator possesses gapless excitations only at its edge in the form of a one-dimensional (1D) helical channel,^{4,5)} a WTI accommodates low-energy electrons arising from helical edge channels only on its side surface. We refer to such surface electrons as Dirac electrons since they obey the massless Dirac equation in the low-energy limit. Notably, low-energy surface states of WTIs typically consist of two Dirac cones in the reciprocal space. Although disorder-induced scattering between two Dirac cones is not forbidden, it does not necessarily extinguish the topological nature of WTIs.^{6–16)} Several materials have been proposed as possible WTIs.^{17–21)}

A characteristic feature of Dirac electrons shows up when a perpendicular magnetic field is applied. Dirac electrons are quantized into Landau levels following the unique quantization rule that the energy of the n th Landau level is proportional to $\sqrt{2n}$.²²⁾ This has been experimentally observed in strong topological insulators,^{23,24)} as in graphene.²⁵⁾ Several authors have theoretically studied how the Landau levels are formed on a surface of strong topological insulators.^{26–29)} However, an attempt similar to this has been lacking for Dirac electrons in WTIs. In this paper, we study the Landau quantization of Dirac electrons on a side surface of WTIs in the presence of a perpendicular magnetic field. To describe Dirac electrons in a magnetic field, we mainly employ an effective 2D Hamiltonian composed of coupled 1D chains of helical edge channels.^{14,15,30)} It has been

demonstrated³⁰⁾ that this effective 2D model can be derived from a 3D Wilson-Dirac Hamiltonian for bulk topological insulators.²⁶⁾ We partly employ this 3D Hamiltonian to confirm the validity of the 2D Hamiltonian. The central question of this study is: does the Landau quantization in WTIs reveal a unique behavior arising from the characteristic features of the system under consideration? The answer is yes. If the side surface is infinitely long as we assume below, Landau levels are specified by the index n and the wave number k_y in the longitudinal direction. In the weak magnetic field regime where the magnetic length l_B is much larger than the interlayer distance a , the behavior of the Landau level is basically explained within the ordinary quantization rule for Dirac electrons. However, a nontrivial behavior appears with decreasing l_B toward a . We find that, when l_B/a becomes sufficiently small, each Landau level and its spin state are modulated in an oscillatory manner as a function of $l_B^2 k_y/a$ with period 1 and the modulation becomes pronounced with increasing index n . We demonstrate that this nontrivial behavior is attributed to the mixing of two Dirac cones induced by the discreteness of the layered structure of WTIs.

In the next section, we present the effective 2D Hamiltonian as well as the 3D Wilson-Dirac Hamiltonian, and briefly explain the relationship between them. In Sec. 3, we present the massless Dirac equation that is derived from the 2D Hamiltonian in the continuum limit. The quantization rule for Dirac electrons is derived on its basis. In Sec. 4, we numerically determine the band structure of Dirac electrons and calculate the spin expectation value of lower quantized levels for several magnetic field strengths. We find that each Landau level and its spin state become modulated in a nontrivial manner with decreasing l_B toward a . In Sec. 5, we present an explana-

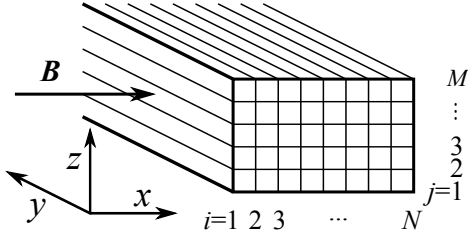


Fig. 1. Structure of a WTI sample considered in the text; it consists of M layers in the z -direction with $M \geq j \geq 1$ and N sites in the x -direction with $N \geq i \geq 1$, while it is infinitely long in the y -direction. A magnetic field \mathbf{B} is applied perpendicularly to the side surface on the yz -plane.

tion for the nontrivial behavior. Section 6 is devoted to a summary and discussion. We set $\hbar = 1$ throughout this paper.

2. Model

Let us consider a WTI sample that consists of M layers in the z -direction and N sites in the x -direction, while it is infinitely long in the y -direction (see Fig. 1). Let j be the index used to specify the M layers, each of which is regarded as a 2D QSH insulator. The N sites in the x -direction are specified by the index i . We assume that low-energy Dirac electrons emerge on the side surfaces of height M in the yz -plane at $i = 1$ and N . If N is chosen to be sufficiently large, the low-energy states on one surface and those on the other surface are mutually independent and exactly degenerate. Thus, we hereafter consider only the side surface at $i = 1$. Let $|j\rangle_\uparrow$ and $|j\rangle_\downarrow$ respectively be the basis vectors for right-going and left-going branches of the 1D helical channel arising from the j th QSH layer. Under the translational invariance in the y -direction, surface electron states are characterized by the wave number k_y . The effective 2D Hamiltonian for Dirac electrons on the side surface is given by^{14, 15, 30)}

$$H_{2D} = \sum_{j=1}^M |j\rangle \begin{bmatrix} vk_y & 0 \\ 0 & -vk_y \end{bmatrix} \langle j| + \sum_{j=1}^{M-1} \left\{ |j+1\rangle \begin{bmatrix} 0 & -\frac{1}{2a}v' \\ \frac{1}{2a}v' & 0 \end{bmatrix} \langle j| + \text{h.c.} \right\}, \quad (1)$$

where $|j\rangle \equiv \{|j\rangle_\uparrow, |j\rangle_\downarrow\}$ and a is the lattice constant, which is simply the interlayer distance. In this model, the Dirac points appear at $(k_y, k_z) = (0, 0)$ and $(0, \pi/a)$. For convenience, we define the z -coordinate of the j th chain as

$$z_j = \left(j - \frac{M+1}{2} \right) a \quad (2)$$

by setting the origin (i.e., $z = 0$) at the center of the system. A perpendicular magnetic field $\mathbf{B} = (B, 0, 0)$ is introduced in terms of the vector potential $\mathbf{A} = (0, A_y, 0)$

with

$$A_y = -Bz. \quad (3)$$

With this choice of \mathbf{A} , the wave number k_y remains a good quantum number since the translational invariance in the y -direction is preserved. The effect of \mathbf{B} can be taken into account by replacing k_y in the Hamiltonian with $k_y + eA_y$. The Zeeman term is ignored in the main part of our analysis, and its effect is briefly discussed in Sec. 6.

To supplement H_{2D} , we also use the 3D Wilson-Dirac Hamiltonian for topological insulators:²⁶⁾

$$H_{3D} = \begin{bmatrix} M_{\mathbf{k}} & A_{\perp} k_z a & 0 & A_{\parallel} k_{-a} \\ A_{\perp} k_z a & -M_{\mathbf{k}} & A_{\parallel} k_{-a} & 0 \\ 0 & A_{\parallel} k_{+a} & M_{\mathbf{k}} & -A_{\perp} k_z a \\ A_{\parallel} k_{+a} & 0 & -A_{\perp} k_z a & -M_{\mathbf{k}} \end{bmatrix}, \quad (4)$$

where $k_{\pm} = k_x \pm ik_y$ and

$$M_{\mathbf{k}} = m_0 + m_{2\parallel}(k_x^2 + k_y^2)a^2 + m_{2\perp}k_z^2a^2. \quad (5)$$

We discretize the x - and z -coordinates and implement H_{3D} on the square lattice in the xz -plane leaving the y -coordinate unchanged.³⁰⁾ In accordance with our assumption that the system is equivalent to 2D QSH insulators stacked in the z -direction, we focus on the weak topological phase with $\boldsymbol{\nu} \equiv (001)$. After the discretization, the Wilson mass term $M_{\mathbf{k}}$ is modified to

$$M_{\mathbf{k}}^{\text{dis}} = m_0 + m_{2\parallel} \{ 2[1 - \cos(k_x a)] + (k_y a)^2 \} + m_{2\perp} 2[1 - \cos(k_z a)]. \quad (6)$$

The weak topological phase with $\boldsymbol{\nu} \equiv (001)$ is stabilized when the parameters satisfy¹¹⁾

$$m_{2\parallel} > \frac{1}{4}|m_0| > m_{2\perp} > \frac{1}{4}|m_0| - m_{2\parallel}, \quad (7)$$

where $m_{2\parallel} > 0 > m_0$ is assumed. This condition fixes the sign of the mass term at four symmetric points on the $k_x k_z$ -plane with $k_y = 0$ as follows:

$$M_{\mathbf{k}}^{\text{dis}} = \begin{cases} m_0 < 0, & \mathbf{k}' = (0, 0) \\ m_0 + 4m_{2\parallel} > 0, & \mathbf{k}' = (\pi/a, 0) \\ m_0 + 4m_{2\perp} < 0, & \mathbf{k}' = (0, \pi/a) \\ m_0 + 4m_{2\parallel} + 4m_{2\perp} > 0, & \mathbf{k}' = (\pi/a, \pi/a) \end{cases}, \quad (8)$$

where $\mathbf{k}' = (k_x, k_z)$. This indicates that, on the side surface in the yz -plane, the Dirac point appears at $(k_y, k_z) = (0, 0)$ and $(0, \pi/a)$ in accordance with the 2D model. Again, the effect of \mathbf{B} can be taken into account by the replacement of k_y with $k_y + eA_y$.

It should be pointed out that the 2D model can be derived from the 3D model.³⁰⁾ The velocities in the 2D model are directly related to the parameters of the 3D model,

$$v = A_{\parallel} a, \quad (9)$$

$$v' = A_{\perp} a. \quad (10)$$

3. Continuum Dirac Theory

Let us consider the effective 2D Hamiltonian given in Eq. (1) in the continuum limit. Note that our model involves the two Dirac cones. Hereafter, the Dirac cones centered at $(k_y, k_z) = (0, 0)$ and $(0, \pi/a)$ are respectively referred to as the first and second Dirac cones. In the continuum limit, the effective Hamiltonians H_+ and H_- describing low-energy states in the first and second Dirac cones are given by

$$H_{\pm} = \begin{bmatrix} v(k_y - eBz) & \mp v' \partial_z \\ \pm v' \partial_z & -v(k_y - eBz) \end{bmatrix}, \quad (11)$$

where the vector potential is explicitly included. It is convenient to parameterize the strength of B in terms of the magnetic length defined by

$$l_B = \frac{1}{\sqrt{eB}}. \quad (12)$$

The anisotropy of the system is characterized by

$$r = \frac{v'}{v}. \quad (13)$$

We determine the eigenstates of H_{\pm} by using the annihilation and creation operators satisfying the commutation relation of $[a, a^{\dagger}] = 1$, defined by

$$a = \frac{\tilde{l}_B}{\sqrt{2}} \left[\frac{1}{\tilde{l}_B^2} (z - z_c(k_y)) + \partial_z \right], \quad (14)$$

$$a^{\dagger} = \frac{\tilde{l}_B}{\sqrt{2}} \left[\frac{1}{\tilde{l}_B^2} (z - z_c(k_y)) - \partial_z \right], \quad (15)$$

where $\tilde{l}_B = \sqrt{r} l_B$ and $z_c(k_y) = l_B^2 k_y$. With these operators, H_{\pm} is rewritten as

$$H_{\pm} = \frac{\sqrt{r}v}{\sqrt{2}l_B} \begin{bmatrix} -(a + a^{\dagger}) & \mp (a - a^{\dagger}) \\ \pm (a - a^{\dagger}) & (a + a^{\dagger}) \end{bmatrix}. \quad (16)$$

The eigenvalues are quantized into the Landau levels as

$$E_{\pm n} = \pm \frac{\sqrt{r}v}{l_B} \sqrt{2n} \quad (17)$$

with $n \geq 0$. The wave functions are expressed in terms of the eigenstates of the number operator $a^{\dagger}a$ satisfying

$$a^{\dagger}a\psi_n(z) = n\psi_n(z), \quad (18)$$

where the explicit forms of the lower three functions are given by

$$\psi_0(z) = \frac{1}{\sqrt{\pi \tilde{l}_B}} e^{-\frac{(z - z_c(k_y))^2}{2\tilde{l}_B^2}}, \quad (19)$$

$$\psi_1(z) = \frac{\sqrt{2}}{\sqrt{\pi \tilde{l}_B}} \left(\frac{z - z_c(k_y)}{\tilde{l}_B} \right) e^{-\frac{(z - z_c(k_y))^2}{2\tilde{l}_B^2}}, \quad (20)$$

$$\psi_2(z) = \frac{\sqrt{2}}{\sqrt{\pi \tilde{l}_B}} \left[\left(\frac{z - z_c(k_y)}{\tilde{l}_B} \right)^2 - \frac{1}{2} \right] e^{-\frac{(z - z_c(k_y))^2}{2\tilde{l}_B^2}}. \quad (21)$$

Note that $\psi_n(z)$ depends on k_y since it is centered at $z_c(k_y)$. The eigenstate of H_+ with the energy $E_{\pm n}$ is expressed as

$$\phi_{\pm n}^+(z) = \frac{1}{2} \begin{bmatrix} \psi_n(z) \mp \psi_{n-1}(z) \\ \psi_n(z) \pm \psi_{n-1}(z) \end{bmatrix} \quad (22)$$

for $n > 0$ and

$$\phi_0^+(z) = \frac{1}{\sqrt{2}} \begin{bmatrix} \psi_0(z) \\ \psi_0(z) \end{bmatrix}. \quad (23)$$

The eigenstate of H_- with the energy $E_{\pm n}$ is expressed as

$$\phi_{\pm n}^-(z) = \frac{1}{2} \begin{bmatrix} \psi_n(z) \mp \psi_{n-1}(z) \\ -\psi_n(z) \mp \psi_{n-1}(z) \end{bmatrix} \quad (24)$$

for $n > 0$ and

$$\phi_0^-(z) = \frac{1}{\sqrt{2}} \begin{bmatrix} \psi_0(z) \\ -\psi_0(z) \end{bmatrix}. \quad (25)$$

The spin state of ϕ_m^{\pm} with $m = 0, \pm 1, \pm 2, \dots$ is determined by the expectation value of the Pauli spin matrices,

$$\langle \phi_m^{\pm} | \boldsymbol{\sigma} | \phi_m^{\pm} \rangle = \int dz [\phi_m^{\pm}(z)]^{\dagger} \boldsymbol{\sigma} \phi_m^{\pm}(z). \quad (26)$$

We easily obtain

$$\langle \phi_m^{\pm} | \boldsymbol{\sigma} | \phi_m^{\pm} \rangle = (0, 0, 0) \quad (27)$$

for $m \neq 0$ and

$$\langle \phi_0^{\pm} | \boldsymbol{\sigma} | \phi_0^{\pm} \rangle = (\pm 1, 0, 0). \quad (28)$$

The above argument provides the quantization rule for Dirac electrons in WTIs. Firstly, the energy of the n th Landau level is quantized into a value proportional to $\sqrt{2n}$, as in monolayer graphene.^{22, 25} Secondly, each Landau level is doubly degenerate, reflecting the existence of the two Dirac cones. Thirdly, the Landau levels are not spin-polarized except for the 0th Landau level $\phi_0^{\pm}(z)$, which is polarized to the $\pm x$ -direction. This rule is reliable when $l_B/a \gg 1$.

4. Numerical Results

We numerically determine the band structure of Dirac electrons in the presence of a perpendicular magnetic field on the basis of the effective 2D Hamiltonian H_{2D} . We also calculate the expectation values of z and $\boldsymbol{\sigma}$ to observe whether the quantization rule obtained from the continuum Dirac theory is applicable even in a strong magnetic field.

Figure 2 shows the band structure of the system with $r \equiv v'/v = 0.4$ and $M = 21$. We see that several dispersion-less flat subbands appear in a restricted region of k_y . They correspond to Landau levels. Inside the dis-

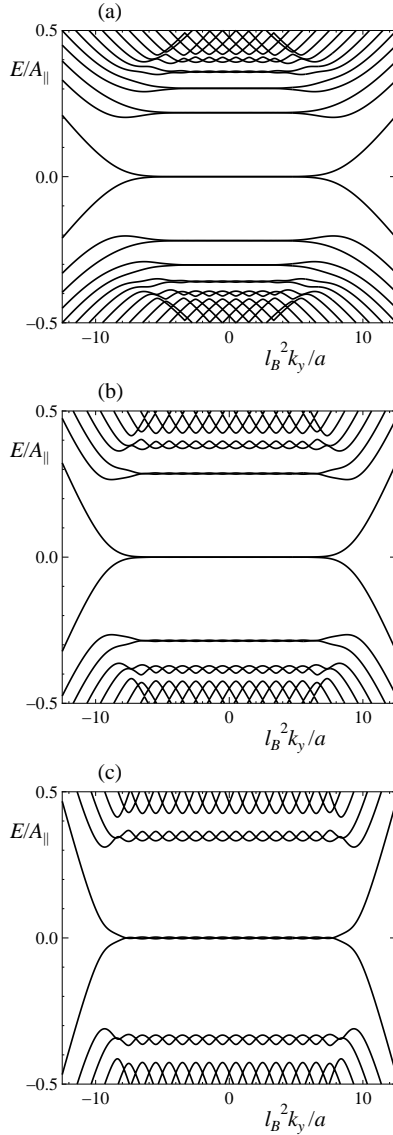


Fig. 2. Band structures in the cases of (a) $l_B/a = 4$, (b) $l_B/a = 3$, and (c) $l_B/a = 2.4$ with $r = 0.4$ and $M = 21$.

played energy range of $|E/A_{\parallel}| \leq 0.5$, we can identify the Landau levels with the indices $n = 0, \pm 1, \pm 2, \pm 3$, and ± 4 in the weak magnetic field case of $l_B/a = 4$. In the stronger case of $l_B/a = 3$, the Landau levels with $n = \pm 3$ and ± 4 cannot be identified. Note that our system is restricted to the finite width of $(M-1)a/2 \geq |z|$. Thus, roughly speaking, the Landau levels with a small n stably exist under the condition of $(M-1)/2 - l_B/a \gtrsim l_B^2|k_y|/a$ as $\psi_n(z)$ is centered at $z_c = l_B^2 k_y$ and its spatial range is on the order of l_B .³¹⁾ In the case of $M = 21$ and $l_B/a = 4$, the condition is simplified to $6 \gtrsim l_B^2|k_y|/a$, in good agreement with the result shown in Fig. 2. Outside of this region, each energy level shows a dispersion as a function of k_y . This suggests the appearance of chiral edge states. We also see that each Landau level is dou-

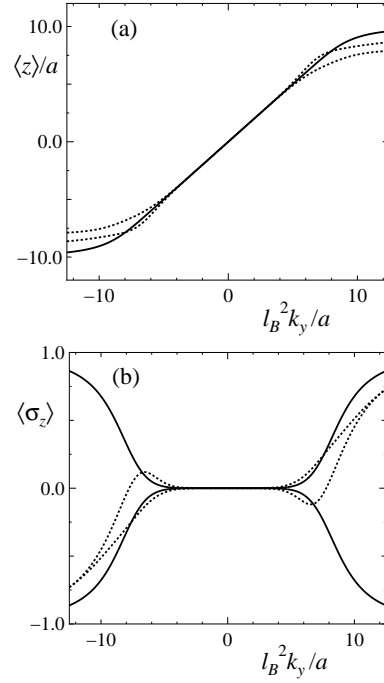


Fig. 3. Expectation values in the case of $l_B/a = 4$ with $r = 0.4$ and $M = 21$: (a) $\langle z \rangle/a$ and (b) $\langle \sigma_z \rangle$ in the 0th Landau level (solid line) and in the 1st Landau level (dotted line).

bly degenerate, reflecting the existence of the two Dirac cones. A peculiar feature of the Landau levels shown in Fig. 2 is that they deviate from the flat dispersion and are modulated in an oscillatory manner as a function of $l_B^2 k_y/a$ with a period of 1. This becomes pronounced with decreasing l_B and/or increasing the index n . The oscillatory behavior cannot be explained within the continuum Dirac theory.

Figure 3 shows the expectation values of z and σ_z in the 0th and 1st Landau levels in the case of $l_B/a = 4$ with $r = 0.4$ and $M = 21$. We see that $\langle z \rangle/a$ is proportional to k_y in the central region of $6 \gtrsim l_B^2|k_y|/a$. Outside of this region, $\langle z \rangle/a$ approaches the edge position (i.e., ± 10) with increasing $|k_y|$, indicating the appearance of chiral edge states. This is also confirmed by the result of $\langle \sigma_z \rangle$ in the region of $l_B^2|k_y|/a \gtrsim 10$, indicating that the spin is polarized to the $\pm z$ -direction (i.e., $\langle \sigma_z \rangle \sim \pm 1$) with increasing $|k_y|$. As an edge state going to the positive (negative) direction is mainly composed of spin-up (spin-down) channels near the corresponding edge of the system, its spin should be polarized to the z -direction ($-z$ -direction). In the central region of $6 \gtrsim l_B^2|k_y|/a$, $\langle \sigma_z \rangle$ vanishes in accordance with the continuum Dirac theory. The expectation value of σ_x as well as that of σ_y vanishes not only in the 1st Landau level but also in the 0th Landau level regardless of k_y (data not shown). This is in contrast to the prediction of the continuum Dirac theory (i.e., the 0th Landau level is spin-polarized to the

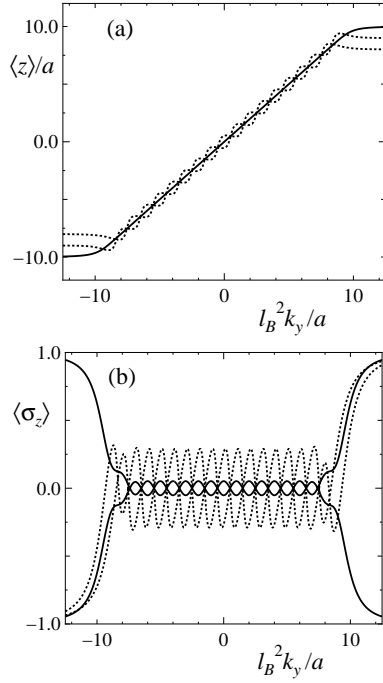


Fig. 4. Expectation values in the case of $l_B/a = 2.4$ with $r = 0.4$ and $M = 21$: (a) $\langle z \rangle/a$ and (b) $\langle \sigma_z \rangle$ in the 0th Landau level (solid line) and in the 1st Landau level (dotted line).

$\pm x$ -direction), implying that the corresponding states in the first and second Dirac cones are hybridized to form spin-unpolarized states.

Figure 4 shows the expectation values of z and σ_z in the 0th and 1st Landau levels in the case of $l_B/a = 2.4$ with $r = 0.4$ and $M = 21$. We see that $\langle \sigma_z \rangle$ oscillates as a function of $l_B^2 k_y/a$ with a period of 1. In the 1st Landau level, $\langle z \rangle/a$ also shows an oscillatory behavior. These features cannot be explained within the continuum Dirac theory.

One may think that the 2D model becomes unreliable with decreasing l_B and the oscillatory behavior shown above is an artifact induced by an erroneous application of the 2D model. In the remainder of this section, we show that this hypothesis can be ruled out. To show this, we calculate the band structure in the case of much stronger magnetic fields by using both the 2D model and the 3D model. In determining the band structure on the basis of H_{3D} , we consider an infinitely long rectangular prism-shaped system of height M and width N (see Fig. 1). Setting $M = 21$ and $N = 20$, we numerically determine the band structure with the following parameters: $A_\perp/A_\parallel = 0.4$, $m_0/A_\parallel = -0.6$, $m_{2\parallel}/A_\parallel = 0.5$, $m_{2\perp}/A_\parallel = -0.1$. Figure 5 shows the band structures obtained from the 2D and 3D models in the cases of $l_B/a = 2$ and 1. The results are almost identical with each other. This supports the reliability of H_{2D} even in a strong magnetic field.

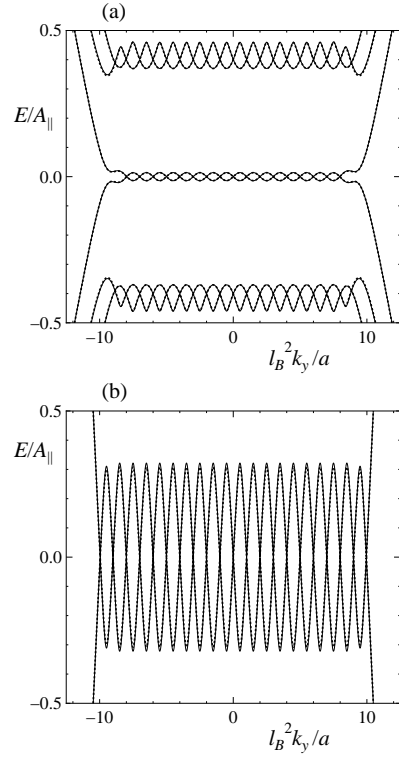


Fig. 5. Band structures in the cases of (a) $l_B/a = 2$ and (b) $l_B/a = 1$ with $r = 0.4$ and $M = 21$, where solid and dotted lines, respectively representing the results of the 2D and 3D models, almost completely overlap with each other.

5. Beyond the Continuum Dirac Theory

In the previous section, we observed the nontrivial behavior of the Landau level that cannot be explained within the continuum Dirac theory. We can consider that this reflects the bare character of 1D helical channels constituting surface states of WTIs, as explained below.

As a transparent example, let us focus on the subband corresponding to the 0th Landau level. If the mutual coupling of 1D helical channels is ignored, the energy of the j th channel disconnected from neighboring ones is

$$\epsilon_{j\sigma} = \sigma v \left(k_y - \frac{z_j}{l_B^2} \right) \quad (29)$$

under the choice of \mathbf{A} given in Eq. (3), where $\sigma = +$ for the spin-up state and $\sigma = -$ for the spin-down state. Hence, at

$$\frac{l_B^2 k_y}{a} = \frac{z_j}{a} = j - \frac{M-1}{2}, \quad (30)$$

the energy of the j th channel is $\epsilon_{j\sigma} = 0$ regardless of its spin state while that of the nearest-neighbor channels is $\epsilon_{j\pm 1\sigma} = \mp \sigma v a / l_B^2$. Thus, we see that the coupling of the j th helical channel to the $j+1$ th and $j-1$ th channels becomes weak with decreasing l_B/a . This indicates that, in the vicinity of $l_B^2 k_y/a = z_j/a$, the subband

state is governed by the j th channel if l_B/a is sufficiently small, resulting in nearly linear energy dispersions. This behavior is most clearly observed in the case of $l_B/a = 1$ shown in Fig. 5(b). Generally speaking, the coupling of 1D helical channels is effectively weakened by an applied magnetic field and, as a result, the character of nearly disconnected 1D helical channels manifests itself when l_B/a is sufficiently small.

The explanation given above is based on an approach from the strong magnetic field limit. An alternative approach from the weak magnetic field limit is also possible. We show below that the nontrivial behavior observed in the previous section is explained within the continuum Dirac theory by adding a correction that induces the mixing of the two Dirac cones. Our attention is focused on surface states located near the center of the system, and thus chiral edge states are beyond our consideration below.

We start with the approximate solutions of the eigenvalue equation for H_{2D} , defined by

$$|\phi_{\pm n}^+\rangle = \sqrt{a} \sum_j |j\rangle \phi_{\pm n}^+(z_j), \quad (31)$$

$$|\phi_{\pm n}^-\rangle = \sqrt{a} \sum_j |j\rangle e^{i\pi j} \phi_{\pm n}^-(z_j), \quad (32)$$

where the factor $e^{i\pi j}$ is attached to $|\phi_{\pm n}^-\rangle$ since it belongs to the second Dirac cone centered at $(k_y, k_z) = (0, \pi/a)$. In the limit of $l_B \gg a$, they satisfy $H_{2D}|\phi_{\pm n}^{\pm}\rangle = E_{\pm n}|\phi_{\pm n}^{\pm}\rangle$ as well as the orthonormalization condition of $\langle \phi_{\pm n}^{\alpha} | \phi_{\pm n'}^{\alpha'} \rangle = \delta_{\alpha, \alpha'} \delta_{n, n'}$ with $\alpha, \alpha' = +$ or $-$. However, with decreasing l_B toward a , these equations are satisfied only in an approximate sense. Note that the term representing electron transfer between neighboring chains in H_{2D} is approximated by the derivative with respect to z in the Dirac theory. This approximation becomes worse with decreasing l_B . Let us consider a correction for this approximation.

For definiteness, we consider the n th Landau level with $E_n \geq 0$ consisting of $|\phi_n^+\rangle$ in the first Dirac cone and $|\phi_n^-\rangle$ in the second Dirac cone, and evaluate the energy deviation from E_n by taking account of only the hybridization between them. Since $\phi_n^{\pm}(z)$ is the solution of the Dirac equation, $|\phi_n^{\pm}\rangle$ satisfies

$$(H_{2D} - E_n) |\phi_n^{\pm}\rangle = \pm i \frac{v'}{2a} \sqrt{a} \sum_j |j\rangle \sigma_y P_j^{\pm} \times [2a \partial_z \phi_n^{\pm}(z_j) - \phi_n^{\pm}(z_{j+1}) + \phi_n^{\pm}(z_{j-1})], \quad (33)$$

where $P_j^+ = 1$ and $P_j^- = e^{i\pi j}$. The right-hand side of Eq. (33), including the difference between the derivative and the finite difference, represents the error of the continuum approximation. If $\langle \phi_n^{\alpha} | \phi_n^{\alpha'} \rangle = \delta_{\alpha, \alpha'}$ is assumed, we obtain

$$\langle \phi_n^{\pm} | H_{2D} | \phi_n^{\pm} \rangle = E_n + \delta_n, \quad (34)$$

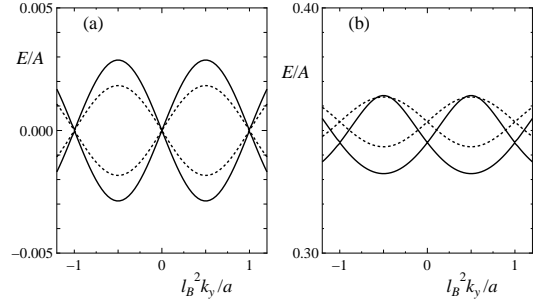


Fig. 6. k_y dependence of the energy of the n th Landau level in the case of $l_B/a = 2.4$ for (a) $n = 0$ and (b) $n = 1$, where solid lines represent the result obtained from H_{2D} while dotted lines represent Eq. (41).

$$\langle \phi_n^{\pm} | H_{2D} | \phi_n^{\mp} \rangle = \gamma_n \quad (35)$$

with

$$\delta_n = \frac{v'}{4} \sum_j (K_j^{n, n-1} - K_j^{n-1, n}), \quad (36)$$

$$\gamma_n = \frac{v'}{4} \sum_j e^{i\pi j} (K_j^{n, n} - K_j^{n-1, n-1}) \quad (37)$$

for $n > 0$ and

$$\delta_0 = 0, \quad (38)$$

$$\gamma_0 = \frac{v'}{2} \sum_j e^{i\pi j} K_j^{0,0}, \quad (39)$$

where

$$K_j^{n,m} = \psi_n(z_j) [2a \partial_z \psi_m(z_j) - \psi_m(z_{j+1}) + \psi_m(z_{j-1})]. \quad (40)$$

δ_n and γ_n appear to represent the correction arising from the discreteness of the layered structure. Note that they depend on k_y as $\psi_n(z_j)$ is centered at $z_c = l_B^2 k_y$. Diagonalizing the 2×2 matrix composed of Eqs. (34) and (35), we find that the energy is shifted to

$$E_n^{\pm}(k_y) = E_n + \delta_n(k_y) \pm \gamma_n(k_y). \quad (41)$$

In Fig. 6, Eq. (41) is compared with the energy of the n th Landau level obtained from H_{2D} in the case of $l_B/a = 2.4$ for $n = 0$ and 1. We see that the modulation of the energy is roughly explained within this treatment. Since γ_n as well as δ_n is proportional to the difference between the derivative and the finite difference, it becomes large with increasing n . This accounts for the observation that the modulation becomes pronounced with increasing index n of the Landau level. The absence of quantitative agreement implies that the coupling between the Landau levels with different indices is also important.

The eigenstate corresponding to E_n^\pm is obtained as

$$|\Phi_n^\pm\rangle = \sqrt{a} \sum_j |j\rangle \frac{1}{\sqrt{2}} [\phi_n^+(z_j) \pm (-1)^j \phi_n^-(z_j)], \quad (42)$$

which results in

$$|\Phi_n^+\rangle = \frac{\sqrt{a}}{2\sqrt{2}} \sum_j |j\rangle \times \begin{bmatrix} (1 + (-1)^j) (\psi_n(z_j) - \psi_{n-1}(z_j)) \\ (1 - (-1)^j) (\psi_n(z_j) + \psi_{n-1}(z_j)) \end{bmatrix}, \quad (43)$$

$$|\Phi_n^-\rangle = \frac{\sqrt{a}}{2\sqrt{2}} \sum_j |j\rangle \times \begin{bmatrix} (1 - (-1)^j) (\psi_n(z_j) - \psi_{n-1}(z_j)) \\ (1 + (-1)^j) (\psi_n(z_j) + \psi_{n-1}(z_j)) \end{bmatrix} \quad (44)$$

for $n > 0$ and

$$|\Phi_0^+\rangle = \frac{\sqrt{a}}{2} \sum_j |j\rangle \begin{bmatrix} (1 + (-1)^j) \psi_0(z_j) \\ (1 - (-1)^j) \psi_0(z_j) \end{bmatrix}, \quad (45)$$

$$|\Phi_0^-\rangle = \frac{\sqrt{a}}{2} \sum_j |j\rangle \begin{bmatrix} (1 - (-1)^j) \psi_0(z_j) \\ (1 + (-1)^j) \psi_0(z_j) \end{bmatrix}. \quad (46)$$

The above expressions indicate that in $|\Phi_n^+\rangle$, the spin alternately polarizes to the z -direction in the chain with an even j and to the $-z$ -direction in the chain with an odd j , and the direction of spin polarization is completely reversed in $|\Phi_n^-\rangle$. Owing to this oscillatory behavior of the spin direction, the spin state is not polarized owing to self-averaging unless l_B is very small. This accounts for the absence of spin polarization in the case of $l_B/a = 4$ [see Fig. 3(b)]. If l_B decreases to a smaller value, self-averaging becomes ineffective and the spin tends to polarize to the $+z$ - or $-z$ -direction depending on whether the corresponding wave function is dominant on the chains with an even j or those with an odd j . This accounts for the appearance of oscillatory spin polarization in the case of $l_B/a = 2.4$ [see Fig. 4(b)].

The alternating behavior of $|\Phi_n^\pm\rangle$ is very natural because H_{2D} allows a spin-up (spin-down) 1D channel to couple with only neighboring spin-down (spin-up) channels. That is, each eigenstate of H_{2D} should be represented by the superposition of helical channels with their spin direction alternately flipping from chain to chain. This is precisely the feature represented by Eqs. (43)–(46).

Let us consider the strong magnetic field regime where l_B/a is sufficiently small, focusing on the 0th Landau level. The spatial range of the superposition is on the order of l_B , so $|\Phi_0^\pm\rangle$ is dominated by the channel nearest to the center of the wave function. This indicates that our argument based on the continuum Dirac theory is continuously connected to the picture of nearly disconnected helical channels argued in the beginning of this section.

6. Summary and Discussion

In this paper, we have studied how Dirac electrons on a surface of weak topological insulators are quantized into Landau levels in the presence of a perpendicular magnetic field B . When B is sufficiently weak with $l_B/a \gg 1$, the ordinary Landau level structure with dispersion-less flat subbands is observed in accordance with the quantization rule for Dirac electrons. The spin state of each level is not polarized except for chiral edge states appearing near the edges. With increasing B , as $l_B/a \rightarrow 1$, each flat subband becomes oscillating as a function of $l_B^2 k_y/a$ with period 1. The corresponding spin state also becomes oscillating with the same period. We have shown that this nontrivial behavior is attributed to the mixing of the two Dirac cones induced by the discreteness of the layered structure. Alternatively, it can be regarded as a manifestation of the character of a 1D helical channel nearly disconnected from neighboring ones by a magnetic field. We have also shown that these two explanations are consistent with each other.

Here, we discuss the possibility of detecting the nontrivial behavior of the Landau level in actual experimental situations. As its simplest consequence, we expect the broadening of each Landau level, which will be detectable if its width is sufficiently large. When a magnetic field of B [T] is applied, the magnetic length is expressed as $l_B = 25.65/\sqrt{B}$ [nm]. While the magnetic field of $B = 40$ T yields $l_B \approx 4.06$ nm, the interlayer distance of the possible weak topological insulator $\text{KHgSb}^{17)}$ is $a \approx 1.9$ nm. These parameters yield $l_B/a \approx 2.1$. From Fig. 2(c) for the case of $l_B/a = 2.4$ and Fig. 5(a) for the case of $l_B/a = 2$, we see that this value would result in sufficiently large level broadening for its detection. Similar broadening would also appear in monolayer graphene.^{32–34)} However, an extremely strong magnetic field is necessary to detect it as the lattice constant of graphene is on the order of 1 Å.

In the presence of disorder, a further consideration is needed as disorder also induces level broadening. Roughly speaking, the broadening due to disorder is proportional to $l_B^{-1} \propto \sqrt{B}$ and is independent of the index n .³⁵⁾ Hence, the broadening due to disorder slowly increases with increasing B , while the oscillation-induced broadening rapidly increases in the strong magnetic field regime, as can be seen from Figs. 2 and 5. Furthermore, the former is independent of the index n while the latter becomes large with increasing n . We expect that these qualitative differences enable us to detect the oscillation-induced broadening as long as the disorder is not so strong.

So far, the Zeeman effect on Landau levels has been ignored in our argument. Here, we briefly consider it within the continuum Dirac theory. If we take into account the Zeeman term for a magnetic field $\mathbf{B} = (B, 0, 0)$, the

Hamiltonian H_{\pm} becomes

$$\tilde{H}_{\pm} = \begin{bmatrix} v(k_y - eBz) & \mp v'\partial_z + \Delta \\ \pm v'\partial_z + \Delta & -v(k_y - eBz) \end{bmatrix} \quad (47)$$

with

$$\Delta = \frac{1}{2}\mu_B g B, \quad (48)$$

where μ_B and g are respectively the Bohr magneton and the effective g factor. In the presence of the Zeeman term, the energy of the n th Landau level is modified as

$$\tilde{E}_{\pm n} = \pm \frac{\sqrt{rv}}{l_B} \sqrt{2(n + \tilde{\Delta}^2)}, \quad (49)$$

where

$$\tilde{\Delta} = \frac{l_B}{\sqrt{2rv}} \Delta. \quad (50)$$

If $v = 3 \text{ eV}\text{\AA}$ is assumed, we find that $\tilde{\Delta} \approx 0.011g/\sqrt{r}$ at $B = 40 \text{ T}$. The above argument implies that the Zeeman effect induces only a small shift of each quantized level and does not strongly alter the qualitative behavior of the magnetic field effect on Landau levels.

Let us finally examine the stability of surface states against an increase in the magnetic field. For definiteness, we consider the 0th Landau level in the vicinity of $l_B^2 k_y/a = z_j/a$. The corresponding wave function is centered at the j th chain and its spatial range is on the order of l_B . A plausible criterion to ensure its stability is that all helical channels within the distance of l_B from the j th chain stably exist. Equations (6) and (8) indicate that this is ensured under the condition of

$$\tilde{m}_0 + m_{2\parallel} \left(\frac{a}{l_B} \right)^2 < 0 \quad (51)$$

with $\tilde{m}_0 = \max\{m_0, m_0 + 4m_{2\perp}\}$, where $m_{2\parallel} > 0 > \tilde{m}_0$ is assumed. It is convenient to define the characteristic length l_B^c as $l_B^c/a \equiv (m_{2\parallel}/|\tilde{m}_0|)^{1/2}$. If $l_B > l_B^c$, condition (51) is satisfied, resulting in the stabilization of the surface state. However, this does not mean that the surface state completely disappears when $l_B^c > l_B$. Even in this regime, the helical channel in the j th chain persists and its energy is zero at $l_B^2 k_y/a = z_j/a$, but helical channels in its neighboring chains within the distance of l_B are partly or fully destabilized and are replaced with bulk states. As a consequence, the persistent j th helical channel is inevitably coupled with such bulk states. Hence, although the resulting state contains the j th helical channel, it cannot be regarded as a pure surface state.

Acknowledgment

The author thanks T. Arita for technical assistance in numerical computations. This work was supported by a Grant-in-Aid for Scientific Research (C) (No. 15K05130).

- 1) L. Fu, C. L. Kane, and E. J. Mele, Phys. Rev. Lett. **98**, 106803 (2007).
- 2) J. E. Moore and L. Balents, Phys. Rev. B **75**, 121306 (2007).
- 3) R. Roy, Phys. Rev. B **79**, 195322 (2009).
- 4) C. L. Kane and E. J. Mele, Phys. Rev. Lett. **95**, 146802 (2005).
- 5) B. A. Bernevig and S.-C. Zhang, Phys. Rev. Lett. **96**, 106802 (2006).
- 6) Y. Ran, Y. Zhang, and A. Vishwanath, Nat. Phys. **5**, 298 (2009).
- 7) K.-I. Imura, Y. Takane, and A. Tanaka, Phys. Rev. B **84**, 195406 (2011).
- 8) Z. Ringel, Y. E. Kraus, and A. Stern, Phys. Rev. B **86**, 045102 (2012).
- 9) R. S. K. Mong, J. H. Bardarson, and J. E. Moore, Phys. Rev. Lett. **108**, 076804 (2012).
- 10) C.-X. Liu, X.-L. Qi, and S.-C. Zhang, Physica E **44**, 906 (2012).
- 11) K.-I. Imura, M. Okamoto, Y. Yoshimura, Y. Takane, and T. Ohtsuki, Phys. Rev. B **86**, 245436 (2012).
- 12) Y. Yoshimura, A. Matsumoto, Y. Takane, and K.-I. Imura, Phys. Rev. B **88**, 045408 (2013).
- 13) K. Kobayashi, T. Ohtsuki, and K.-I. Imura, Phys. Rev. Lett. **110**, 236803 (2013).
- 14) T. Morimoto and A. Furusaki, Phys. Rev. B **89**, 035117 (2014).
- 15) H. Obuse, S. Ryu, A. Furusaki, and C. Mudry, Phys. Rev. B **89**, 155315 (2014).
- 16) Y. Takane, J. Phys. Soc. Jpn. **83**, 103706 (2014).
- 17) B.-H. Yan, L. Muehler, and C. Felser, Phys. Rev. Lett. **109**, 116406 (2012).
- 18) B. Rasche, A. Isaeva, M. Ruck, S. Borisenko, V. Zabolotnyy, B. Buchner, K. Koepf, C. Ortix, M. Richter, and J. van den Brink, Nat. Mater. **12**, 422 (2013).
- 19) P. Tang, B. Yan, W. Cao, S.-C. Wu, C. Felser, and W. Duan, Phys. Rev. B **89**, 041409 (2014).
- 20) G. Yang, J. Liu, L. Fu, W. Duan, and C. Liu, Phys. Rev. B **89**, 085312 (2014).
- 21) C. Pauly, B. Rasche, K. Koepf, M. Liebmann, M. Pratzner, M. Richter, J. Kellner, M. Eschbach, B. Kaufmann, L. Plucinski, C. M. Schneider, M. Ruck, J. van den Brink, and M. Morgenstern, Nat. Phys. **11**, 338 (2015).
- 22) N. H. Shon and T. Ando, J. Phys. Soc. Jpn. **67**, 2421 (1998).
- 23) P. Cheng, C. Song, T. Zhang, Y. Zhang, Y. Wang, J.-F. Jia, J. Wang, Y. Wang, B.-F. Zhu, X. Chen, X. Ma, K. He, L. Wang, X. Dai, Z. Fang, X. Xie, X.-L. Qi, C.-X. Liu, S.-C. Zhang, and Q.-K. Xue, Phys. Rev. Lett. **105**, 076801 (2010).
- 24) T. Hanaguri, K. Igarashi, M. Kawamura, H. Takagi, and T. Sasagawa, Phys. Rev. B **82**, 081305 (2010).
- 25) K. S. Novoselov, A. K. Geim, S. V. Morozov, D. Jiang, M. I. Katsnelson, I. V. Grigorieva, S. V. Dubonos, and A. A. Firsov, Nature **438**, 197 (2005).
- 26) C.-X. Liu, X.-L. Qi, H. Zhang, X. Dai, Z. Fang, and S.-C. Zhang, Phys. Rev. B **82**, 045122 (2010).
- 27) Z. Yang and J.-H. Han, Phys. Rev. B **83**, 045415 (2011).
- 28) R. Ilan, F. de Juan, and J. E. Moore, arXiv:1410.5823.
- 29) T. Morimoto, A. Furusaki, and N. Nagaosa, Phys. Rev. Lett. **114**, 146803 (2015).
- 30) T. Arita and Y. Takane, J. Phys. Soc. Jpn. **83**, 124716 (2014).
- 31) More precisely speaking, the spatial range of $\psi_n(z)$ is on the order of $\sqrt{n+1/2}l_B$, so the n th Landau level stably exists under the condition of $(M-1)/2 - \sqrt{n+1/2}l_B/a \gtrsim l_B^2|k_y|/a$.
- 32) K. Wakabayashi, M. Fujita, H. Ajiki, and M. Sgrist, Phys. Rev. B **59**, 8271 (1999).
- 33) Y. Hasegawa and M. Kohmoto, Phys. Rev. B **74**, 155415 (2006).
- 34) Y. Hatsugai, T. Fukui, and H. Aoki, Phys. Rev. B **74**, 205414 (2006).
- 35) M. Koshino and T. Ando, Phys. Rev. B **75**, 235333 (2007).